Creation of Optical Vortices Using an Adjustable Spiral Phase Plate and Computer-Generated Holograms

Physics Individual Project
Siemens-Westinghouse Competition
October 2005

Amol Jain

Herricks High School
New Hyde Park, New York 11040

and

Laser Teaching Center
Stony Brook University

Abstract

An adjustable spiral phase plate and computer-generated holograms were investigated as methods for creating optical vortices. The phase plate was created by cutting a plastic microscope cover slip from a corner to its center and separating the resultant tabs by inserting a uniformly thick wedge between them. The computer-generated holograms were designed by mathematically interfering an oblique plane wave with an optical vortex in Matlab; we then printed them on common overhead transparencies.

The two devices were tested in an originally developed interferometer, and the intensity profiles of vortices created by shining a laser beam through the phase plate and CGHs were measured. The curvature of the phase plate was mapped using an optical scanning setup. A composite-vortex grid hologram was designed for future use in an orbital angular momentum sorter in conjunction with the spiral phase plate. Both devices simplified previous designs and proved to be a highly effective means of generating optical vortices.

1 Introduction

Vortices are a ubiquitous phenomenon in nature. They have long been observed in hurricanes, tornadoes, and even something as simple as the swirl of coffee in a mug. It was only in 1974, however, that Berry and Nye first put forth the theory that a light field could assume the character of a vortex [1]. Since then, optical vortices have become more than a mathematical curiosity and have proved their practical value in numerous fields, including optical tweezing and quantum computation [2].

An optical vortex beam is characterized by a doughnut-shaped intensity distribution with a phase singularity, and hence zero field amplitude, at the center. Optical vortices feature a screw-shaped topological wavefront dislocation, which can be visualized as a helical phase ramp around the field's dark center. The phase varies linearly with the azimuthal angle ϕ as described by the phase term $\exp[il\phi]$. The annular intensity profile ($l > 0$) provides normalizing forces useful in stabilizing trapped particles, and the spiral phase distribution endows each photon with an orbital angular momentum of $l\hbar$. The orbital angular momentum of an optical vortex is used to apply torques to particles in an optical tweezers setup and, more recently, has served as a medium for encoding information [3].

Two of the most common means of producing optical vortices are spiral phase plates and computer-generated holograms. Spiral phase plates directly impose the vortex structure on an incident beam by linearly varying the optical path length around the circumference of the device. Computer generated holograms (CGHs) are created by mathematically interfering an oblique plane wave with an optical vortex and function by diffracting a plane wave into multiple orders of optical vortices of distinct topological charge. CGHs can also be used to determine a vortex's topological charge.

In the current research simple and inexpensive designs for spiral phase plates and CGHs were implemented and further simplified, and a composite-vortex grid CGH was created for future use in an orbital angular momentum sorter. This paper includes a discussion the theory behind the function of these devices and an analysis of their performance and efficacy.

2 Theory

2.1 Optical Vortices

2.1.1 The Fundamental Gaussian

The geometry of a laser cavity determines the gain material that will be used to produce the beam. The distinct beams that develop, or modes, are solutions to the complex wave equation:

$$\nabla^2 U - \frac{1}{c^2}\frac{\partial^2 U}{\partial t^2} = 0$$

Generally, several modes will compete for the gain material with one dominant but oscillating mode. Commercial lasers are usually designed to suppress modes other than the fundamental Gaussian, which minimizes fluctuations, tightens the beam waist, and betters the beam quality.

The fundamental mode is a specific solution to the wave equation, and it may be described:

$$U_0(r,z) = \frac{1}{w}\exp\left[-\frac{ikr^2}{2R} - \frac{r^2}{w^2} - i\psi\right]$$

where $R(z) = z\sqrt{1+(z/z_0)^2}$ is the wave-front radius of curvature, $w(z) = w_0\sqrt{1+(z/z_0)^2}$ is the beam radius, and ψ is the Guoy phase.

2.1.2 The Laguerre-Gaussian

Traces of the equation above are evident in the function that describes a Laguerre-Gaussian beam, or optical vortex [5]. In fact, the zeroth order LG beam simplifies to a pure Gaussian.

$$U_l^p(r,\phi,z) = \exp\left[-\frac{ikr^2}{2R} - \frac{r^2}{w^2} - i(2p+l+1)\psi\right]\exp[-il\phi](-1)^p\left(\frac{r^2}{w^2}\right)^{\frac{l}{2}} L_p^l\left(\frac{2r^2}{w^2}\right)$$

where L_n^k is a generalized Laguerre polynomial:

$$L_n^k(x) = \sum_{m=0}^{n} (-1)^m \frac{(n+k)!}{(n-m)!(k+m)!m!} x^m$$

The two indices of the mode are l and p which describe the total phase change around the circumference of the vortex ($2\pi l$) and the number of radial maxima ($p+1$), respectively. For the purposes of this discussion, all beams will be assumed to have $p = 0$.

The distinguishing characteristic of optical vortices is found in the $\exp[il\phi]$. The angle ϕ resides in the plane transverse to the direction of beam propagation and introduces the element of azimuthal variance in LG beams. As ϕ varies from 0 to 2π, the phase of light around the circumference is calculated by $l\phi$. A suitable analogy is found in the Earth. If we are to look down upon the north pole, we would see lines of longitude (indicative of the azimuthal angle and, hence, the phase of light) converging upon the center. At the north pole, there is no distinct longitude. Likewise, at the center of an optical vortex, there is a singularity in the phase, and the amplitude of the beam is necessarily zero. This gives rise to optical vortices' dark center and doughnut shaped intensity distribution.

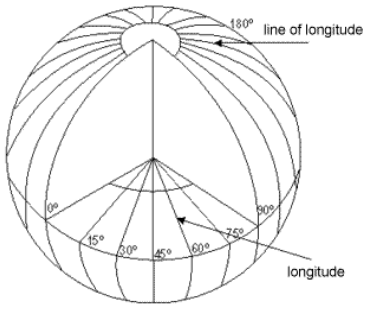

Figure 1: Comparison between the phase in a cross section of an optical vortex and longitude lines at the north pole

The topological charge of a vortex is another name for its l-value. If we are to connect all points of equal phase in a charge one vortex, we would create a helical phase ramp. The locus of points of equal phase in a charge two vortex would produce a double-helix. The trend holds true for larger l. The radius of an optical vortex increases with l.

2.2 Methods of Production

Common methods for producing optical vortices include intra-cavity circular absorbers, astigmatic mode converters, computer-generated holograms (CGHs), and spiral phase plates. Intra-cavity circular absorbers significantly reduce the intensity of the beam and require access to the laser cavity, rendering them impractical for use in many circumstances. Astigmatic mode converters rely on high-order Hermite-Gaussian modes of certain indices [6], making them more cumbersome to set up. This research focuses the two latter methods of production: CGHs and spiral phase plates.

2.3 Spiral Phase Plates

2.3.1 Traditional phase plates

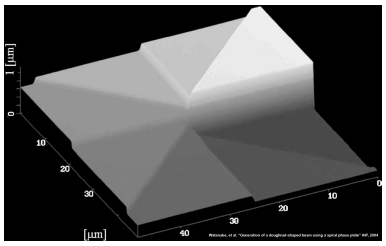

Figure 2: The increasing thickness translates to an increased optical path length and, thus, a phase shift

Spiral phase plates function by directly imposing a phase shift on the incident light. They are constructed from a piece of transparent material with gradually increasing, spiraling thickness. Light slows down in optically dense media, taking more time to cover a given distance inside the media than outside in air. It simplifies matters, however, to approach phase shift in terms of distance rather than time. Thus we define the idea of the optical path length, the apparent distance light travels in any medium:

$$\Lambda = \int n(s)ds$$

where n, the index of refraction, is a function of distance s. The thicker the plate, the longer the optical path length, and the greater the phase shift. The spiraling thickness of a phase plate creates the spiraling phase distribution of an optical vortex. In order to be effective, the phase plate must be smooth and accurately shaped to a fraction of a wavelength. Furthermore, even if it is successfully produced, it is only applicable to one wavelength of light and one topological charge.

2.3.2 Adjustable spiral phase plates

A more versatile means of creating optical vortices is an adjustable spiral phase plate [7]. These phase plates can be used with multiple wavelengths and produce a range of topological charges. They were created by twisting a piece of cracked Plexiglas and orienting the device so that one tab of the phase plate was directly perpendicular to the incident light, and the other tab was bent at some angle θ away from the other. A laser directed at the end of the crack will then produce an optical vortex because of the azimuthally varying tilt around the center of the phase plate.

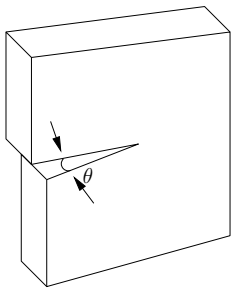

Figure 3: The two sides of the crack in the phase plate are separated by an angle θ

2.3.3 Optical Path Length as a Function of Tilt

Tilting any transparent object with two parallel sides causes a change in optical path length. The derivation is slightly elusive, but we finally found the relationship between tilt angle and change in optical path length as follows.

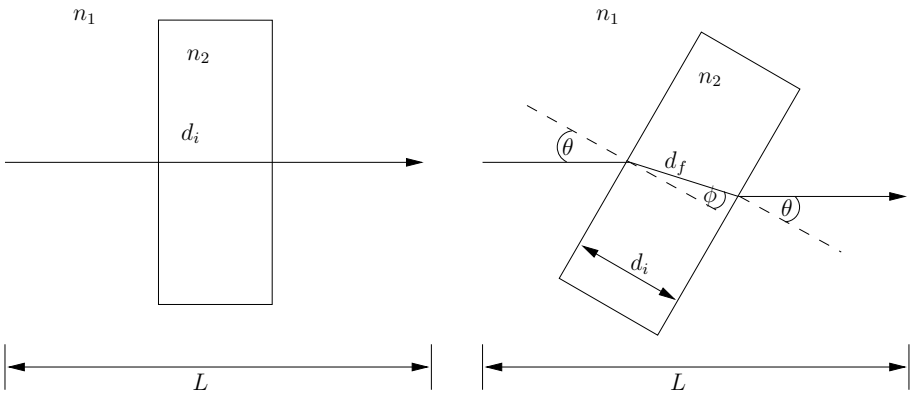

Figure 4: Change in optical path length due to a rotating transparent medium with parallel sides

Over the course of some distance L, light must pass through two different media: air (n_1) and the transparent medium (n_2), where $n_2 > n_1$. Let us consider the first case of the un-rotated plate. The distance traveled in air is simply $l_i = L - d_i$, and the distance in the medium, $d_i = d_i$ (d_i is defined to be the width of the plate). The second case is slightly more complex. A second angle ϕ is introduced such that, by Snell's law:

$$\sin\phi = \frac{n_1 \sin\theta}{n_2}$$

The distance traveled in air must compensate for the effects of refraction:

$$l_f = L - d_f \cos(\theta - \phi)$$

As does the distance in the medium:

$$d_f = \frac{d_i}{\cos(\phi)}$$

The change in optical path length is then described by:

$$\Delta\Lambda = (l_f n_1 + d_f n_2) - (l_i n_1 + d_i n_2)$$

Substituting and rearranging, we achieve this equation, which will be used later to analyze the experimental spiral phase plate:

$$\Delta\Lambda = d_i \left[n_1 \left(1 - \frac{\cos(\theta - \phi)}{\cos(\phi)} \right) + n_2 \left(\frac{1}{\cos(\phi)} - 1 \right) \right]$$

2.4 Computer Generated Holograms

2.4.1 Holograms

A picture taken with black and white film records only one facet of a scene: the intensity of light (the square of the amplitude of its electric field). Information about the phase of light, one of the factors that makes objects appear three-dimensional, is completely lost. Holograms offer a means of preserving the phase. In essence, a hologram is just an interference pattern created by a plane reference wave and light scattered off a selected object.

A diffraction grating is created by developing the photoplate, and shining the reference beam through this grating exactly reproduces the light, in intensity and phase, that was initially scattered off the object. Looking through the grating provides the illusion that the original object is truly there.

2.4.2 Forked Gratings

CGHs are used to create optical vortices in precisely the same manner. If we are to record the interference pattern between a plane wave and an optical vortex on a photoplate and later shine the plane reference wave through the grating, we would correctly expect to produce an optical vortex identical to the former one. We can theoretically produce a CGH as follows [8].

The simplest representation of a phase singularity (optical vortex) can be written as

$$E(r, \theta, z) = E_0 \exp(il\theta) \exp(-ikz)$$

where l is the topological charge and θ is an angle in the plane transverse to the direction of propagation. Next, consider a plane wave u, propagating obliquely to the axis

$$u = \exp(-ik_x x - ik_z z)$$

Assume the recording device is located at $z = 0$ for simplicity. The intensity distribution may then be found by squaring the sum of the two amplitude functions:

$$I = 1 + E_0^2 + 2E_0 \cos(k_x x - l\theta)$$

A Fourier transform of this yields the transmittance function actually used to create the diffraction gratings [9].

$$T(r, \theta) = T_0 \exp\left[i\alpha \cos\left(l\theta - \frac{2\pi}{\Lambda} r \cos\theta\right)\right]$$

where α is the amplitude of the phase modulation, T_0 is the constant absorption coefficient of the hologram, and Λ is period of the grating (fringe spacing).

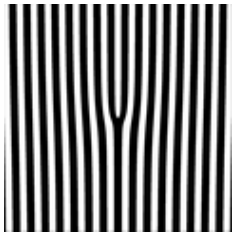

Figure 5: An $l = 1$ grating or the interference pattern created by an oblique plane wave and charge 1 vortex

Interference patterns between plane waves and optical vortices are characterized by a fork in the center. The charge of the vortex can be determined by counting the number of forks, or subtracting one from the number of prongs. Because these are diffraction gratings, shing a plane wave through one of them will actually create multiple vortices of $\{\ldots, -l, 0, +l, \ldots\}$ charge, where the negative charges have the phase ramp in the opposite direction.

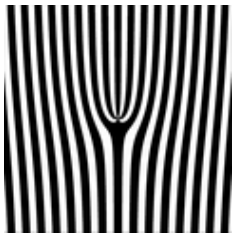

Figure 6: An $l = 4$ grating. Note how there are 4 forks (5 prongs)

3 Experimental Procedure

3.1 Materials

The materials used for creating the devices that generated optical vortices were fairly meager. Plastic cover slips (22 mm square, 0.25 mm thick) were cut to produce an adjustable spiral phase plate. The CGHs were developed in Matlab 7, reduced using ImageMagick and printed at 600dpi on common transparencies.

Equipment used for testing these devices was more extensive. Most important was the Melles Griot HeNe (λ =632.8 nm) laser, output at 30mW. Two 50-50 non-polarizing beam splitters and about a dozen mirrors, all ThorLabs, were used among the interferometer, the surface scanning setup, and the CGH setup. A ThorLabs photodetector, model DET-110, and a digital multimeter were used to experimentally determine the relationship between medium tilt angle and the phase shift. Images and intensity distributions were recorded on either the Sony Mavica or the Powershot SD400 digital cameras.

3.2 Adjustable Spiral Phase Plate

A plastic microscope cover slip was chosen as an alternative material to Plexiglas for the production of a spiral phase plate. Attempts to replicate the Technion's method using Plexiglas proved unsuccessful for a number of reasons. The Plexiglass was extremely difficult to crack in a controlled manner and most fractures ocurred arbitrarily. Even if a desirable crack was stumbled upon, the crack tended to propagate while twisting the material eventually caus-

ing the entire piece of Plexiglas to snap in half. In contrast, a cover slip is an inexpensive, optical-quality material that is easily cut with scissors and manipulated without nearly as much concern over durability or crack propagation as Plexiglas. For the experiment, a cover slip was slit radially from the center to a corner. A holster was designed for keeping the phase plate secure and controlling the angle between the two tabs.

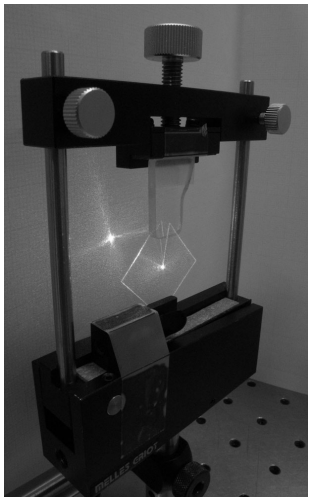

Figure 7: The screw at the top of the holster raises and lowers a piece of Plexiglas into the slit of the cover slip, allowing control over the angle between the two sides

3.2.1 The C.J. Interferometer

The C.J. interferometer was developed independently at the lab and is a hybrid between a Mach-Zehnder and a Sagnac. Its advantage over a Michaelson interferometer is that the laser never retraces its path, so if we put the spiral phase plate in one arm of the device, the laser does not go through it twice, skewing results. The C.J. offers more space than a Sagnac, so placing an object in one arm of the interferometer does not interfere with the path of the laser in the other. Finally, the C.J. allows for more spatial control over the beam than the Mach-Zehnder.

Placing the spiral phase plate in one arm of the interferometer resulted in the forked interference patterns that are characteristic of optical vortices. Turning the screw on the

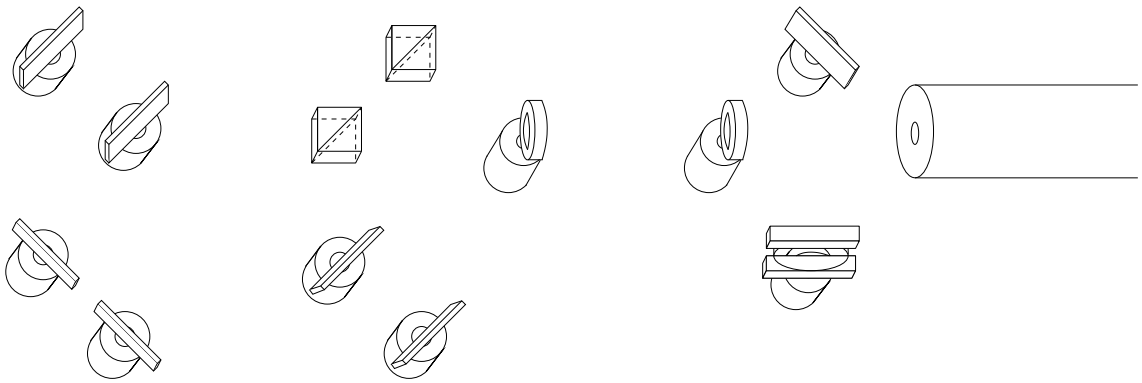

Figure 8: The spiral phase plate is placed in one arm of the C.J. interferometer and the resultant optical vortex is interfered with a plane wave from the other arm

holster clockwise spread the cover slip's slit further apart, and more forks appeared, indicative of higher order vortices. Determining how well the device was working, however, required a better understanding of the surface.

3.2.2 The Surface Scan

The lab equipment for performing a surface scan was quite limited, but the setup, fashioned out of very basic materials, functioned surprisingly well. A lens was placed such that the laser beam, once reflected off of a mirror, came to a focus on the spiral phase plate secured in the holster mounted on a two-dimensional translator. Part of the beam reflected off the phase plate and hit the surface of a Plexiglas screen covered with graph paper. The holster was translated in the horizontal and vertical directions in 0.508 mm (2/100 in) increments over a 10.16 mm by 10.16 mm (0.4 in by 0.4 in) area centered on the middle of the phase plate forming a 21 $\times$ 21 point grid on the cover slip. The position of the laser beam was plotted on the graph paper every time the phase plate was translated. In actuality, only 430 points of data were taken because 11 of the points resided directly on the slit of the phase plate causing the light to scatter.

A process was developed to convert the data on the graph paper into the more meaningful values of the x and y tilt of the spiral phase plate. Figure 12 is a closeup schematic diagram

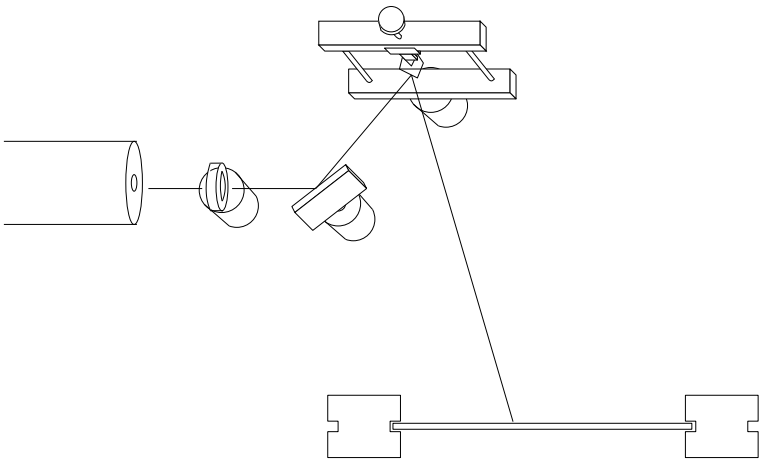

Figure 9: Surface scan experiment

of the laser reflecting off the phase plate, which is tilted at some angle $(\theta_{px}, \theta_{py})$. If $\theta_p x = 0$ (the phase plate is parallel to the initial laser beam and the screen), then the beam will intersect the screen at some x_0, which is used as a reference for all points. Considering the right triangle formed by L, the distance between the phase plate and the screen, and the angle $2\theta_m - 2\theta_{px}$, x, an arbitrary point where the beam falls on the screen, may be defined by

$$x = \frac{L}{\tan(2(\theta_m - \theta_{px}))} - x_0$$

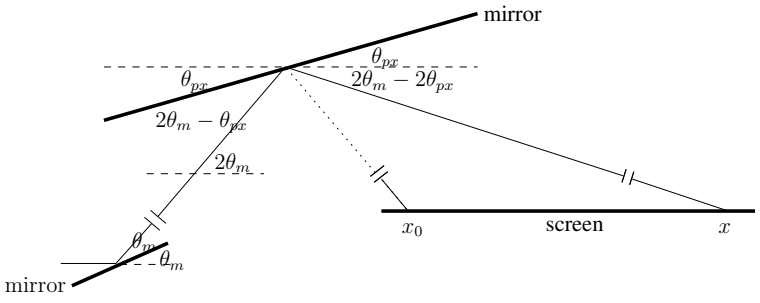

Figure 10: Closeup schematic diagram of laser path during surface scanning

Where the laser intersects the screen in the vertical direction depends upon θ_{px} as well as θ_{py}: the smaller θ_{px} is, the greater the distance before the beam hits the screen, and

consequently, the higher it will hit the screen. Thus y, the vertical coordinate of an arbitrary point where the beam falls on the screen, may be defined by

$$y = \sqrt{L^2 + L^2 \cot^2(2(\theta_m - \theta_{px}))} \tan(\theta_{py})$$

where $\sqrt{L^2 + L^2 \cot^2(2(\theta_m - \theta_{px}))}$ is the length of the beam's path projected onto the plane of the optical table. These two equations yield:

$$\theta_{px} = \theta_m - \frac{1}{2} \tan^{-1}\left(\frac{L}{x + x_0}\right)$$

and

$$\theta_{py} = \tan^{-1}\left(\frac{y}{L\sqrt{1 + \cot^2(2(\theta_m - \theta_{px}))}}\right)$$

The phase shift induced on a light beam depends on the angle between the incident light and the surface normal. Thus, a total tilt θ_t, which describes this angle, is defined as a function of its components θ_x and θ_y by means of a common spherical trigonometric identity to be:

$$\cos(\theta_t) = \cos(\theta_x) \cos(\theta_y)$$

The x and y coordinates of each data point were read off the graph paper and organized in a spreadsheet. All 430 data points were then translated into their total tilt equivalent via the equations above in Matlab.

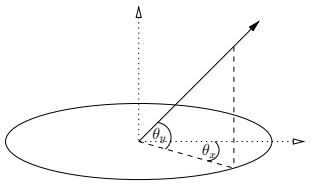

Figure 11: Visualization of θ_x and θ_y

3.2.3 Controlled Tilt Experiment

In order to confirm that the equation relating tilt angle to change in optical path length was derived correctly, an uncut cover slip was placed on a rotation stage in one arm of the interferometer, and the fringes of the interference pattern were projected onto the face of a photodetector. The cover slip was rotated from 90° (perpendicular to the incident light) through 120° at 0.5 degree intervals, and the voltage output from the photodetector was recorded and graphed. Peak voltages indicate the middle of a fringe (a net 2π phase shift, considering the initial 90° position corresponded to the photometer being exposed to the center of a fringe), and voltage minima represent the dark area between fringes (a net $\frac{\pi}{2}$ phase shift). One cycle from peak to peak or trough to trough implies a change of one wavelength in optical path length.

In the equation from section 2.3.3 $\Delta\Lambda$ may be replaced with $m\lambda$, so that the change in optical path length is represented by some m number of wavelengths. Dividing both sides by λ yields an approximately parabolic curve that relates $\Delta\Lambda$ in wavelengths to the tilt angle θ. In order to achieve the cyclical pattern demonstrated by the data, it is only needed to take the cosine of the function and multiply the argument by 2π:

$$p(\theta) = \cos\left(2\pi\frac{d_i}{\lambda}\left[n_1\left(1 - \frac{\cos(\theta-\phi)}{\cos(\phi)}\right) + n_2\left(\frac{1}{\cos(\phi)} - 1\right)\right]\right)$$

The theoretical model fits the experimental graph quite nicely. It is important to note that the more tilted the phase plate was, the less additional rotation was necessary to produce any given phase shift. That is why the data points on each cycle get succesively scarcer. Note that the function actually graphed was $k(l(\theta)) + 1)$, where $k = 8.2$ in order to fit the curve to the voltages measured by the photometer.

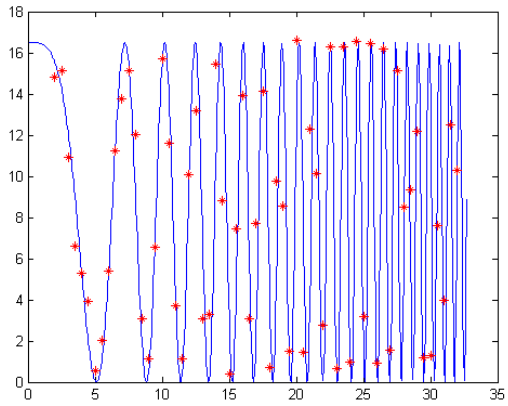

Figure 12: Phaseshift vs. Angle

3.2.4 Phase plate analysis

We used the function above to associate all 430 data points of θ_t with a phase shift in Matlab. The graph on the left is the plot of θ_t against position on the phase plate, and the figure on the right is a map of the phase of light leaving the spiral phase plate. The slit is represented on the left side by a line of 11 uniformly colored squares. The color of the figure is mostly constant along any given radius, confirming that the phase shift is azimuthally dependent(holding the paper farther back may help to see this more easily). A change in color from light to dark to light or dark to light to dark indicates a phase shift of 2π. The phase map suggests that the phase plate is set for creating an $l = 9$ vortex. In the area directly left of the slit, the phase pattern is slightly disordered. Most likely, this may be attributed to irregular twisting of the left tab by the wedge inserted between the two halves.

It is important to note that in order for the phase plate to function, it must be situated such that one tab is directly perpendicular to the incident light, and the other is bent away. This is so the optical path length monotonically increases, resulting on a constantly increasing phase shift around the circumference of the phase plate. If the phase plate was positioned so one tab was bent towards the incoming light and the other tab was bent away at an equal angle, then the vortex phase pattern is destroyed. This was demonstrated by artifically

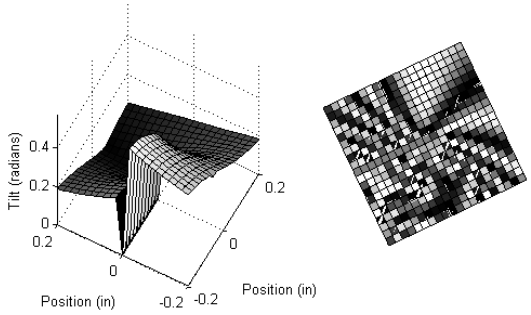

Figure 13: The spiral phase pattern is evident in this phase representation of the area of the phase plate scanned

tilting the phase plate in Matlab so θ_t for both halves of the cover slip were equal.

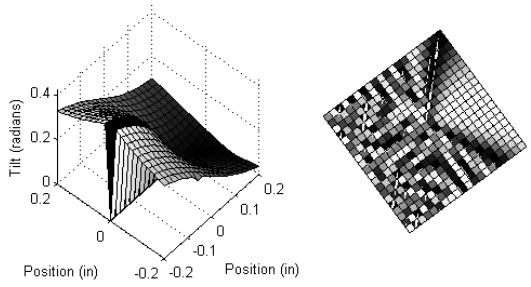

Figure 14: If both sides of the phase plate have the same absolute tilt relative to the incident beam, the vortex pattern is destroyed

It is evident on both sides of the slit that the phase has acquired radial dependence. A path traced from the center to the top left or bottom left corner of the phase map would pass over several changes of phase, a pattern that does not conform to the phase structure of an optical vortex.

3.3 Vortex Analyzer

CGHs are used to create vortices, but they may also be used to analyze them. Shining an optical vortex of the same topological charge as the one used to create the CGH will produce a plane wave. In order to test a beam for its topological charge, one could theoretically shine the beam through an $l = 1$ grating, an $l = 2$ grating, an $l = 3$ grating,... and the grating that produced a plane wave output would correspond to the l-value of the vortex beam. It is possible, however, to speed up this process by using the principle of conservation of topological charge [4], which essentially states that the topological charge of a composite vortex is the sum of the charges of its components. Therefore, one could superimpose two CGHs orthogonally and create composite vortices of a range of topological charges.

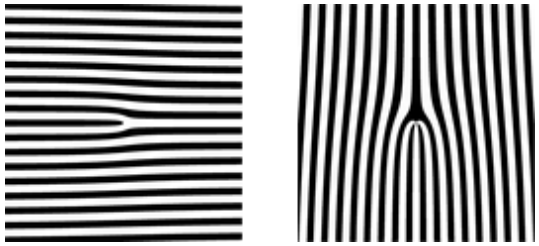

Figure 15: Left: $l = 1$ grating. Right: $l = 3$ grating.

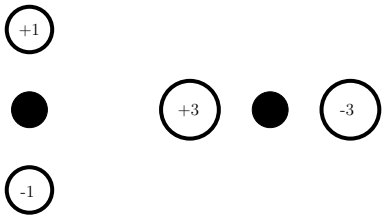

Figure 16: The vortices and their respective topological charges created by the gratings above

Shining a plane wave through Figure 19 would create vortices ranging from $l = -4$ to $l = +4$. As a result, this grating is also capable of analyzing vortices of the same charge range. For example, shining an $l = -3$ vortex through this grid would cause a plane wave beam (Gaussian intensity distribution) to appear in the spot a charge -3 vortex would normally be in under the condition of an incident plane beam.

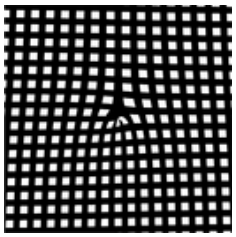

Figure 17: Interference patterns for the $l = 1$ vortex and the $l = 3$ vortex are superimposed to create this grating, which produces composite vortex grids

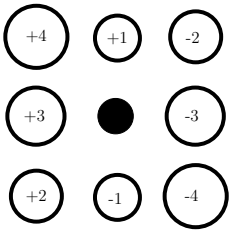

Figure 18: The vortex grid pattern created by the above composite CGH

A modified version of the transmittance function from section 2.4.2 (adjusted for Cartesian coordinates) was used in Matlab to create the above CGHs. The function was calculated for 1800×1800 points in a 16×16 square centered on the origin. The fringe spacing was set to 1. The image created was exported from Matlab and cropped in The Gimp (image editing software) to 2934×2934 pixels. It was reduced to 120×120 pixels in ImageMagick then printed at 10% its size onto common transparency paper at 600dpi by a laser printer.

A previous method for creating CGHs involved taking a film photograph of a large printout of the desired design, then having it developed into a slide from the negatives. This would be a costly and tedious process. It is possible to test grating designs immediately with a device called a spatial light modulator, which can adjust the intensity and/or phase of light using a small, high resolution lcd display, but these cost thousands of dollars. The method developed above is both inexpensive and immediate, and marks a further simplification of the methods used to create optical vortices.

4 Conclusions

The adjustable spiral phase plate constructed from a plastic microscope cover slip was demonstrated to be an effective means of producing optical vortices. The phase distribution of the vortices produced was investigated by performing a surface scan of the phase plate, and conclusions were drawn about the cover slip orientation necessary produce a spiral phase structure. A simplified method for generating optical vortices using computer-generated holograms was also developed and implemented in the form of a composite vortex grid.

Three areas appear promising for future research. First is the construction of an orbital angular momentum sorter [3] capable of encoding information (different l-states) in an optical vortex by a spiral phase plate and decoding information through a composite vortex analyzer similar to the one created above. It would be interesting to see how far apart the encoding and decoding devices could be placed before beam degradation and information corruption. Second is an investigation of amplitude grating efficiencies. Gratings may be blazed to focus the intensity into a particular order vortex or annular to provide cleaner rings [9]. A study of what combinations of modifications would produce an optimal vortex would be very useful. Third is experimenting with optical vortices produced with nonspiral phase plates [10]. Vortices can be generated by linearly phase shifting one half of a laser beam with a curved transparent plate; the simplicity of the method is both highly appealing and intriguing.

References

[1] J. F. Nye, M. V., Berry, "Dislocations in wave trains," *Proc. Roy. Soc. Lond.* A **336**, 165 (1974).

[2] J. Leach, M.J. Padgett, S. M. Barnett, S. Franke-Arnold, J. Courtial, "Measuring the orbital angular momentum of a single photon," *Phys. Rev. Lett.* **88**, 257901 (2002).

[3] G. Gibson, J. Courtial, M.J. Padgett, M. Vasnetsov, V. Pas'ko, S. M. Barnett, and S. Franke-Arnold, "Free-space information transfer using light beams carrying orbital angular momentum," *Opt. Express* **12**, 5448-5456 (2004).

[4] M. S. Soskin, V. N. Gorshkov, M. V. Vasnetsov, J. T. Malos, N. R. Heckenberg, "Topological charge and angular momentum of light beams carrying optical vortices," *Phys. Rev.* A **56**, 4064-4075 (1997).

[5] J. Arlt, K. Dholakia, L. Allen, and M. J. Padgett, "The production of multiringed Laguerre-Gaussian modes by computer-generated holograms," *J. mod. Opt.* **45**, 1231-1237 (1998).

[6] M. W. Beijersbergen, L. Allen, H. E. L. O. van der Veen and J. P. Woerdman, "Astigmatic laser mode converters and transfer of orbital angular momentum," *Opt. Commun.* **96**, 123-132 (1993).

[7] C. Rotschild, S. Zommer, S. Moed, O. Hershcovitz and S. G. Lipson, "Adjustable spiral phase plate," *Appl. Opt.* **43**, 2397-2399 (2004).

[8] H. He, N. R. Heckenberg, H. Rubinsztein-Dunlop, "Optical particle trapping with higer-order doughnut beams produced using high efficiency computer generated holograms," *J. Mod. Opt.* **42**, 217-223 (1995).

[9] C.-S. Guo, X. Liu, X.-Y. Ren, H.-T. Wang, "Optimal annular computer-generated holograms for the generation of optical vortices," *J. opt. Soc. Am.* **22**, 385-390 (2005).

[10] G.-H. Kim, J.-H. Jeon, K.-H. Ko, H.-J. Moon, J.-H. Lee, J.-S. Chang, "Optical vortices produced with a nonspiral phase plate," *Appl. Opt.* **36**, 8614-8621 (1997).